

Star formation properties in the Local Volume galaxies via $H\alpha$ and FUV fluxes.

Igor D. Karachentsev ¹ and Elena I. Kaisina

Special Astrophysical Observatory RAS, Nizhnij Arkhyz, Karachai-Cherkessian Republic,
Russia 369167

ikar@sao.ru, kei@sao.ru

Received _____; accepted _____

¹Leibniz-Institute für Astrophysik (AIP), An der Sternwarte 16, D-14482, Potsdam, Germany

ABSTRACT

A distance-limited sample of 869 objects from the Updated Nearby Galaxy Catalog is used to characterize the star formation status of the Local Volume population. We present a compiled list of 1217 star formation rate (SFR) estimates for 802 galaxies within 11 Mpc from us, derived from the H-alpha imaging surveys and GALEX far-ultraviolet survey. We briefly discuss some basic scaling relations between SFR and luminosity, morphology, HI-mass, surface brightness, as well as environment of the galaxies. About 3/4 of our sample consist of dwarf galaxies, for which we offer a more refined classification. We note that the specific star formation rate of nearly all luminous and dwarf galaxies does not exceed the maximum value: $\log(SFR/L_K) = -9.4$ [yr^{-1}]. The bulk of spiral and blue dwarf galaxies have enough time to generate their stellar mass during the cosmological time, T_0 , with the observed SFRs. They dispose of a sufficient amount of gas to support their present SFRs over the next T_0 term. We note that only a minor part of BCD, Im, and Ir galaxies (about 1/20) proceeds in a mode of vigorous star-burst activity. In general, the star formation history of spiral and blue dwarf galaxies is mainly driven by their internal processes. The present SFRs of E, S0 and dSph galaxies are typically (1/30 - 1/300) of their former activity.

1. Introduction

A series of surveys of nearby galaxies in the $H\alpha$ emission line, determining the star formation characteristics in them was published over the last decade. Typically, the object of study were the galaxies of a fixed morphological type: blue compact galaxies, BCD (Gil de Paz et al. 2003), irregular and BCD (Hunter & Elmegreen, 2004), spiral and irregular

galaxies (James et al. 2004, Epinat et al. 2008), southern objects, rich in neutral hydrogen HI (Meurer et al. 2006), dwarf galaxies in the nearby Sculptor and Centaurus A groups (Bouchard et al. 2009).

The most systematic observations in the $H\alpha$ line were made by Kennicutt et al. (2008), who have selected for their survey the nearby ($D < 11$ Mpc) galaxies with the apparent magnitude $B < 15^m$ at the Galactic latitudes $|b| > 20^\circ$ with the morphological types $T > -1$ in de Vaucouleurs classification. In parallel with this, a program of mass survey of galaxies of the Local Volume (= LV) without any object selection by morphological type was performed at the 6-m BTA telescope of the Russian Academy of Sciences (Karachentsev et al. 2005, Kaisin & Karachentsev 2006, 2008, Kaisin et al. 2007, 2011, Karachentsev & Kaisin 2007, 2010). In total we have obtained the $H\alpha$ -images of more than 300 galaxies with distances of $D < 11$ Mpc within our program. The summary of $H\alpha$ fluxes for more than 500 LV-galaxies was published in the Updated Nearby Galaxy Catalog (= UNGC) (Karachentsev et al. 2013a). The database and atlas of the LV-galaxies (Kaisina et al. 2012), available at <http://www.sao.ru/lv/lvgdb>, contains a lot of $H\alpha$ -images for nearby galaxies, their $H\alpha$ fluxes along with the flux uncertainties, as well as references to the sources of the observables. Actually, our sample contains nearly 2 times more galaxies than the most recent study by Lee et al. (2011), being also much more representative for the early-type objects (E, S0, dSph) and for the low-mass galaxies with $\log(SFR) < -4$.

It should be emphasized that the sample constraint by a fixed distance and minimal sample selectivity during its compilation are very important circumstances that facilitate interpretation of the obtained data. For example, the use of our sample allows to obtain a less biased estimate of the average star formation rate (SFR) in a unit volume at the present epoch ($z = 0$). It is also useful as a reference sample in the analysis of the effects produced by the overdensities in the nearby Virgo and Fornax clusters on the features of

star formation in their galaxies.

An independent possibility of determining the star formation rates in the nearby galaxies by their far-ultraviolet flux ($\lambda_{eff} = 1539\text{\AA}$, $\text{FWHM}=269\text{\AA}$) has appeared with the FUV flux measurements by the GALEX orbital telescope (Gil de Paz et al. 2007, Lee et al. 2009, 2011). The consolidated data of these authors was significantly supplemented by us with integral m_{FUV} magnitudes of galaxies extracted from the NASA Extragalactic Database and then presented in the UNGC (Karachentsev et al. 2013a) and the LVG data base (Kaisina et al. 2012). The sample discussed below is the most representative of all samples to date.

2. The data sample

The UNGC catalog includes 869 galaxies of the northern and southern sky with individual distance estimates of $D < 11$ Mpc or radial velocities relative to the Local Group centroid of $V_{LG} < 600$ km s⁻¹ if the galaxy distance has not been determined. More than 320 galaxies of the sample have distance estimates derived with an accuracy of $\sim 10\%$ by the TRGB luminosity, the luminosity of Cepheids or Supernovae, or via the surface brightness fluctuations in the galaxy. The distances of 370 members of the Local Volume were determined with an accuracy of $\sim 25\%$ from the Tully-Fisher (1977) relation, luminosity of the brightest stars or evident membership of galaxies in the nearby groups. The kinematic distance estimates of nearby galaxies $D = V_{LG}/H_0$, where H_0 is the Hubble parameter are less reliable, because they may contain a significant bias owing to the participation of nearby galaxies in the large-scale flows from the center of the Local Void or towards the Virgo cluster (Tully et al. 2008).

Following Kennicutt (1998), we determined the integral SFR in a galaxy by the linear

relation

$$SFR[M_{\odot}/yr] = 0.945 \cdot 10^9 F_c(H\alpha) \cdot D^2, \quad (1)$$

where $F_c(H\alpha)$ is its integral flux in the $H\alpha$ line [$\text{erg}\cdot\text{cm}^{-2}\cdot\text{s}^{-1}$], corrected for the Galactic and internal extinction $A(H\alpha) = 0.538(A_B^G + A_B^i)$.

The light extinction in our Galaxy A_B^G was estimated according to Schlegel et al. (1998), and internal extinction A_B^i was expressed through the apparent axial ratio of the galaxy a/b :

$$A_B^i = [1.54 + 2.54(\log 2V_m - 2.5)] \log(a/b), \quad (2)$$

if the amplitude of the galaxy rotation V_m exceeded 39 km s^{-1} (Verheijen 2001); for dwarf galaxies with $V_m < 39 \text{ km s}^{-1}$ and for the gas-poor E, S0 galaxies the internal extinction was assumed to be negligible.

According to Lee et al. (2011), the SFR in a galaxy can be expressed in terms of its apparent FUV magnitude m_{FUV} as

$$\log(SFR[M_{\odot} \cdot \text{yr}^{-1}]) = 2.78 - 0.4m_{FUV}^c + 2 \log D \quad (3)$$

accounting for the Galactic and internal extinction

$$m_{FUV}^c = m_{FUV} - 1.93(A_B^G + A_B^i). \quad (4)$$

Note that Kennicutt & Evans (2012) have recently provided a little lower conversion factor between the SFR and the observed $H\alpha$ or FUV flux, what is mainly the result of a different initial mass function and updated stellar population models.

In total, our sample contains 619 galaxies with the SFR values determined from the FUV fluxes, and 98 galaxies with an upper limit corresponding to $m_{FUV} \simeq 23.0^m$. For 461 galaxies of the Local Volume the SFRs are measured from their fluxes in the $H\alpha$ line, and for 41 galaxies only the upper limits of their integral $H\alpha$ flux are known. Among both

subsamples there are 415 galaxies, the SFRs of which can be estimated by two independent methods. This gives the so far largest basis to compare the methods used.

3. Comparison of SFRs from $H\alpha$ and FUV fluxes

Figure 1 represents the ratio of SFRs, determined via $H\alpha$ and FUV fluxes depending on various global parameters of the galaxies. The members of the Local Volume, for which only an upper limit of the flux in $H\alpha$ or FUV is known are shown by empty triangles pointing down or up, respectively. The remaining objects are shown by circles. The top panel of the figure shows the dependence of the SFR ratio on the absolute B-magnitude of the galaxy. The middle panel gives the SFR ratio as a function of the indicative dynamic mass M_{26} determined within the Holmberg’s isophote, 26.5 mag arcsec⁻². The bottom panel shows the ratio of the SFRs as a function of the total mass of hydrogen M_{HI} . The observed scatter of galaxies in the diagrams of Fig. 1 is due to a variety of causes that are both random and systematic.

First of all, a typical uncertainty of the measured $H\alpha$ flux is around (10 - 20)%, as it was noted by Kennicutt et al. (2009) and Karachentsev & Kaisin (2010). A characteristic uncertainty of FUV fluxes derived from the GALEX data is much lower, however, a scatter of FUV extinction in a galaxy can reach about (20 - 40)%, as shown by Lee et al. (2009). If we also take into account the distance measurement errors (10 - 20)%, one would expect a total uncertainty on SFR($H\alpha$)-to-SFR(FUV) ratio to be somewhat within 50%. But Figure 1 demonstrates a much broader scatter.

Let us recall that the flux in the $H\alpha$ line determines the SFR in a galaxy on a short time scale of $\sim 10^7$ years (because of the luminance of O stars), while the FUV flux is mainly formed by less massive stars of B0-B5 types and corresponds to the time scale

of $\sim 10^8$ years. Due to the bursts of star formation particularly significant in the most low-mass dwarfs (Stinson et al. 2007, Skillman 2005), a scatter of the SFR ratios derived by $H\alpha$ and FUV fluxes should increase with decreasing luminosity or mass of the galaxy. This well expected effect is actually observed in all the panels of Fig.1. The examples of galaxies in central parts of which the bursts of star formation have occurred are M 82, NGC 3412, NGC 3593, NGC 4600.

In the transition from normal disk galaxies to diffuse dwarf objects of low surface brightness, a relative error of determining the $H\alpha$ flux usually increases. Here, an underestimation of the integral $H\alpha$ emission due to the loss of the low-contrast component, distributed outside the compact HII-regions can have a systematic effect. On the other hand, the FUV-images of some diffuse dSph galaxies like the Sculptor, AndI, AndII, AndXI, AndXVII may be contaminated by the foreground blue stars of the Milky Way, what leads to a fictitious increase of the FUV flux in the target galaxy. In addition, the optical contours of dwarf galaxies sometimes contain poorly subtracted traces of very red stars, what fictitiously increases the $H\alpha$ flux (probable examples: AndIII, AndV, AndX). There are also rare cases when a large difference in the SFR estimates from $H\alpha$ and FUV fluxes was caused by small emission knots on the periphery of giant galaxies that are accidentally projected onto the images of dwarf satellites. Examples of such cases are KDG61 as a companion to M81 (Karachentsev et al. 2011) and M32 as a companion to M31.

Finally, we point out two instances: DDO 120 = UGC 7408 and NGC 1533, where significant errors in the measured $H\alpha$ flux are caused by a poor control of weather conditions during the observations or problems with data reduction.

In addition to all of the listed circumstances, it must be remembered that the transition from the $H\alpha$ and FUV fluxes to the SFR values is based on the empirical relationships (1) – (4), the validity of which is not entirely justified. Pflamm-Altenburg et al. (2007,

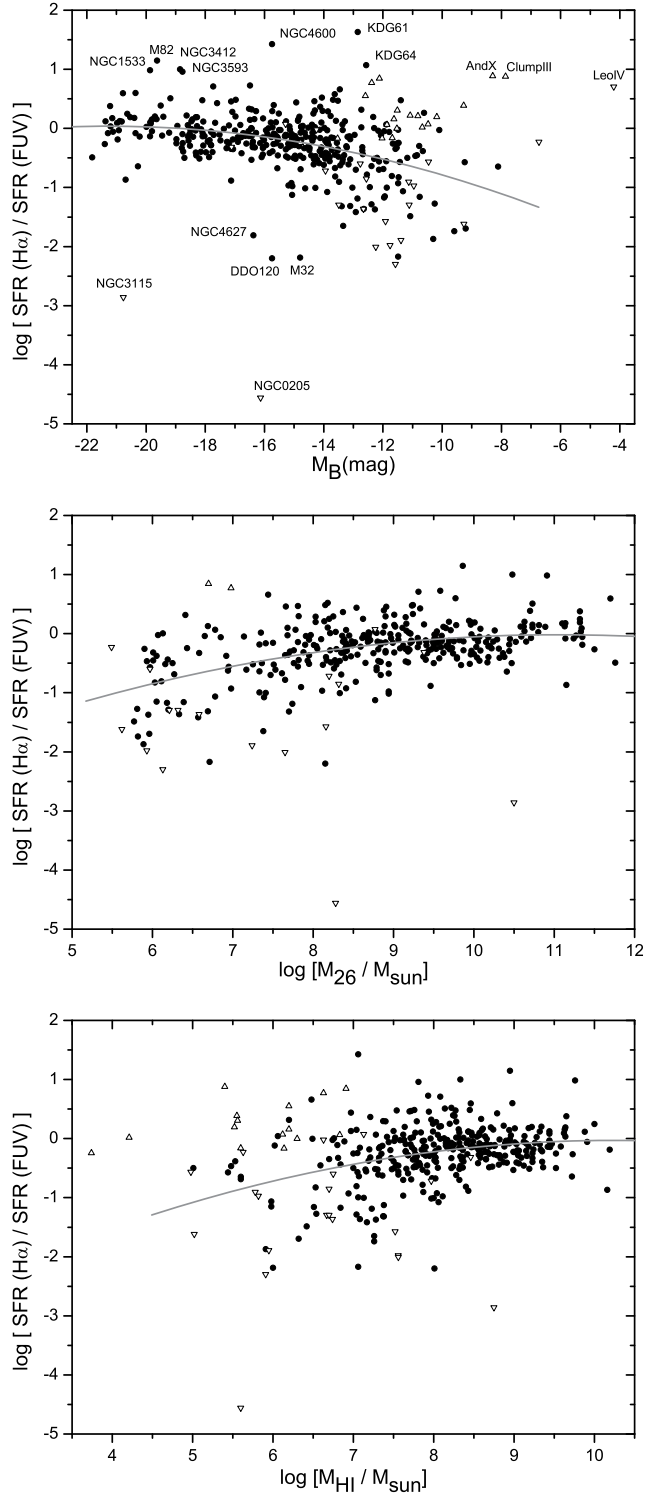


Fig. 1.— The ratio of $H\alpha$ -to-FUV star formation rates as a function of different global galaxy parameters: absolute blue magnitude (top panel), indicative dynamical mass within the Holmberg diameter (middle panel), and total hydrogen mass (bottom panel). The solid lines show the quadratic least squares fits to the data.

2009) placed emphasis on this cardinal problem, according to whom there is a systematic underestimation of SFR in dwarf galaxies from their $H\alpha$ fluxes. The authors see the cause of discrepancy in the features of the initial function of stellar mass in dwarf galaxies (the deficiency of stars of the highest luminosity in them). Detailed discussions on these issues can be found in Lee et al. (2009, 2011), Meurer et al. (2009), Hunter et al. (2010), Fumagelli et al. (2011), Weisz et al. (2012), and Relano et al. (2012). In particular, Fumagelli et al. (2011) suggested that a lower $H\alpha$ -to-FUV flux ratio in dwarf galaxies compared with that in the brighter systems could be explained by the stochastic sampling even for a universal initial mass function. Weisz et al. (2012) considered the effects of a bursty star formation history (SFH) and found a set of SFH models that are well-matched with the observational data, implying that the more massive galaxies have nearly constant SFHs, while the low-mass systems experience burst amplitudes of 10 - 50. Their bursty models are able to reproduce both the observed systematic decline and an increased scatter in the $H\alpha$ -to-FUV ratios towards the low-mass systems.

One reason for the discrepancy between the SFR estimates from the $H\alpha$ and FUV fluxes can be a wrong account of the internal light extinction in the galaxies. To test this reason, we compared the ratio of SFR estimates from $H\alpha$ and FUV fluxes with an apparent axial ratio of galaxies a/b in the logarithmic scale. As the data in the upper panel of Fig. 2 shows, the disk spiral galaxies of morphological types $T=(2-8)$, i.e. $T=(\text{Sa-Sdm})$ have a relatively small scatter of $\log[SFR]_{H\alpha} - \log[SFR]_{FUV}$ with the average value being near zero. Consequently, the semi-empirical relations (1) and (3) are mutually well-calibrated for normal disk galaxies. Some trend of decreasing $[SFR]_{H\alpha}/[SFR]_{FUV}$ towards the galaxies with large inclinations indicates a possible overestimation of the value of internal extinction in the disks by the relations (2) and (4).

For the dwarf galaxies of $T = 9, 10$ morphological types (BCD, Im, Ir), the logarithmic

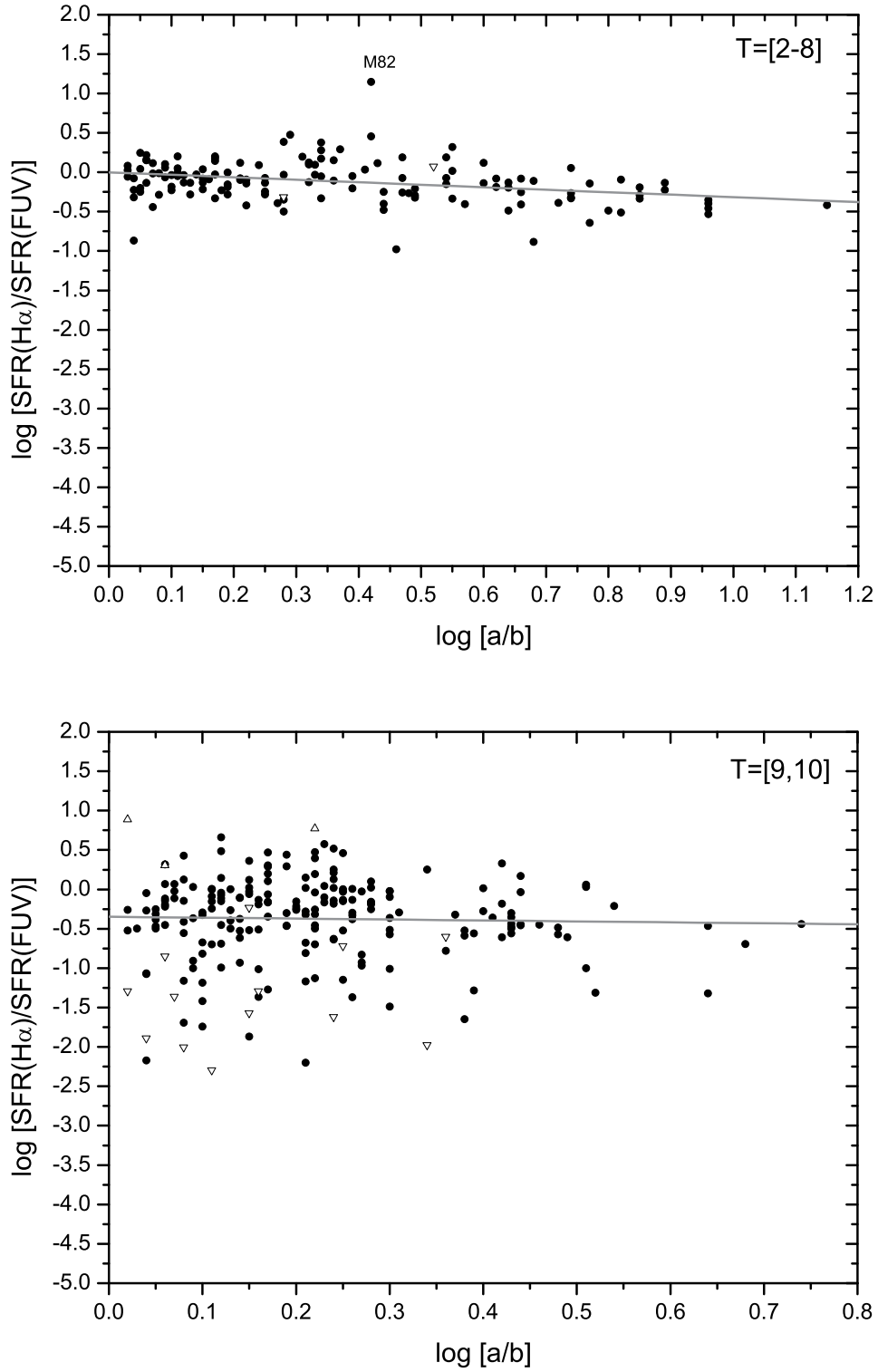


Fig. 2.— The ratio of $H\alpha$ -to-FUV SFRs vs. apparent axial ratio for spiral galaxies (top panel) and late-type irregular dwarfs (bottom panel). The solid lines indicate the linear least squares fits to the data.

difference of SFR estimates is characterized by a significantly greater dispersion. On the average, the value of $[SFR]_{FUV}$ is two times higher than $[SFR]_{H\alpha}$ and is practically independent on the angle of inclination of galaxy. It is interesting to note that the scatter of difference of $\log[SFR]$ shows a decreasing trend from the dwarf galaxies seen face-on to the edge-on ones.

The difference $\log[SFR]_{H\alpha} - \log[SFR]_{FUV}$, depending on the morphological type of galaxies is shown in the upper panel of Fig. 3. As follows from these data, for early-type ($T < 2$) galaxies, the SFR estimates from $H\alpha$ flux are on the average 2–5 times higher than those found from the FUV flux, also showing a large scatter here. It is not entirely clear for us what causes this feature. An average difference between the estimates of $\log[SFR]$ decreases from the early to late types, and their variance is minimal for the spiral disks of $T = (2-5)$, systematically increasing towards the latest types. The reported trends of the SFR estimates via $H\alpha$ and FUV fluxes along the Hubble sequence have not yet obtained a physical interpretation.

Meurer et al. (2009) paid attention to the correlation between $H\alpha$ -to-FUV flux ratio and a galaxy surface brightness. They found that low R- band surface brightness galaxies have lower ratio of the fluxes compared to high surface brightness galaxies. They presented this as the “strongest” evidence for systematic initial mass function variations, supporting the idea proposed by Pflamm-Altenburg et al.(2009). On the bottom panel of Fig. 3 we present the $H\alpha$ -to-FUV SFR ratio versus B- band surface brightness of a galaxy within its Holmberg radius. As one can see, our much more representative sample shows also the mentioned correlation, but only as a slight tendency. The observed noisy trend may be caused by known correlations of the mean surface brightness with other galaxy parameters: luminosity, morphology, HI-content, etc.

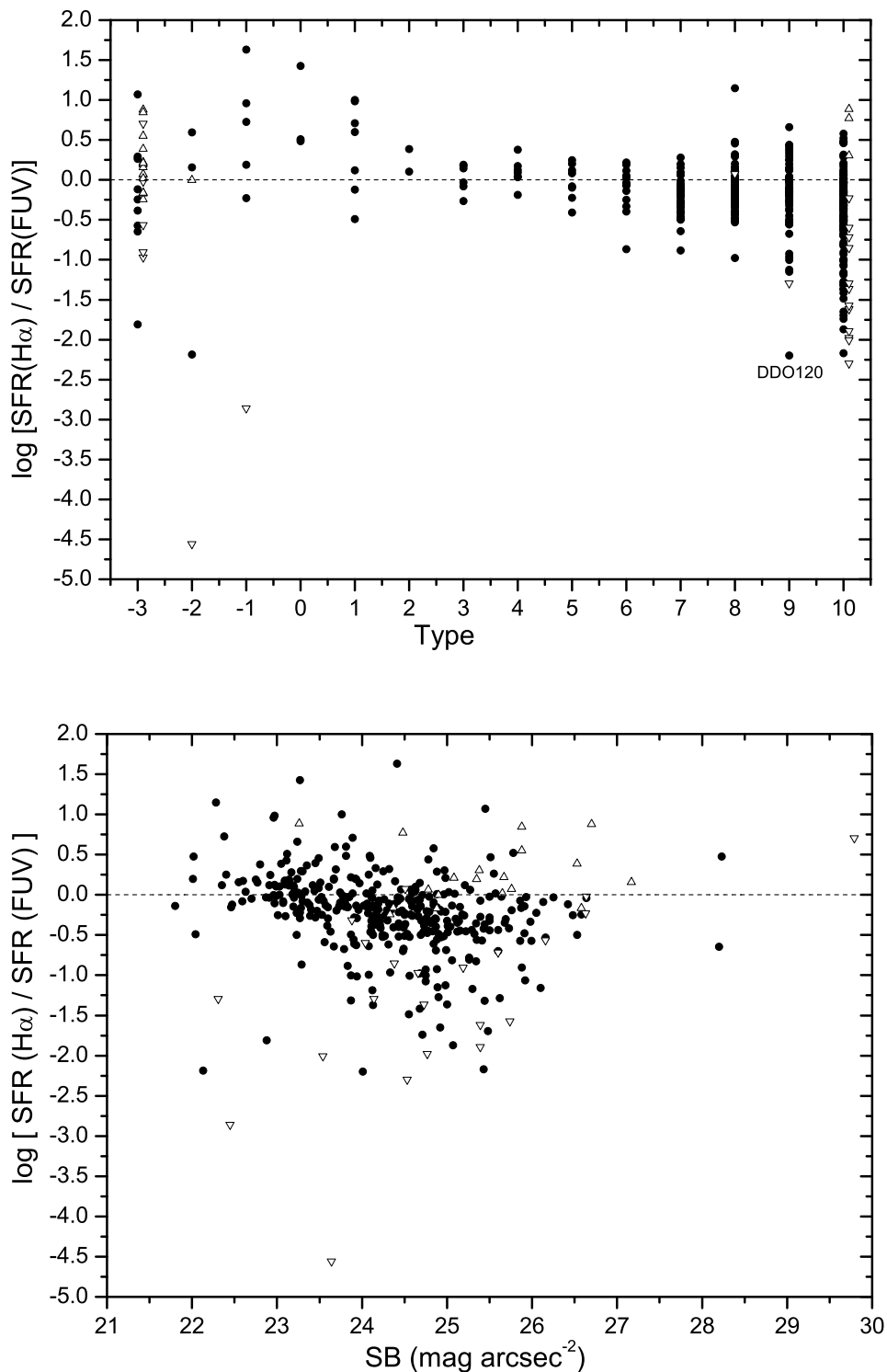


Fig. 3.— The ratio of $H\alpha$ -to-FUV SFRs vs. morphological type of galaxies on de Vaucouleurs scale (upper panel) and vs. the mean B-band surface brightness within the Holmberg radius (bottom panel). The galaxies with upper limit of $H\alpha$ or FUV flux are shown by open triangles directed towards top or bottom, respectively.

4. Some scaling relations

It is well known that integral star formation rate in disk galaxies is approximately proportional to their integral luminosity, i.e. the specific star formation rate per luminosity unit in them is roughly one and the same (Young et al. 1996, Karachentsev & Kaisin 2007, James et al. 2008, Lee et al. 2009). This assertion is true, however, only in the first approximation. In addition to the luminosity, there apparently exist other parameters of galaxies affecting the difference in specific star formation rates (SSFR).

The top panel of Fig. 4 shows the distribution of galaxies in the Local Volume by their SSFR per luminosity unit in the K_s -band and the logarithm of integral K-luminosity. The galaxies with SFRs estimated from the $H\alpha$ and FUV fluxes are depicted by circles and triangles, respectively. Empty symbols denote galaxies with an upper limit of the $H\alpha$ or FUV flux. Since the stellar population of galaxies has an average mass-to-luminosity ratio in the K-band of $\sim 1M_\odot/L_\odot$ (Bell et al. 2003), the L_K -scale actually matches the scale of integral stellar mass of the galaxies, M_* . In this diagram, the galaxies of the Local Volume vary by 8 orders of magnitude in luminosity and 6 orders of magnitude in their SSFRs. In addition to the horizontal "Main Sequence" for disk galaxies, a vertical "column" stands out on the right side of the diagram, which consists of galaxies of the highest luminosity. Most of them are early-type (Sa-Sb) spirals containing a prominent bulge with old population. Different bulge-to-disc fractions in them apparently lead to the observed scatter along the vertical scale. Even greater differences in the specific SFR are revealed in the dwarf galaxies. Only in a minor part they are due to the increase of $H\alpha$ and FUV flux measurement errors in the low-luminosity galaxies near the sensitivity threshold of the $H\alpha$ and FUV surveys. The main reasons of the observed scatter are physical: the sweep-out of gas from the dwarf galaxies during their passage through extended haloes of giant galaxies, and cycles of star formation bursts which are the most significant in low-mass systems.

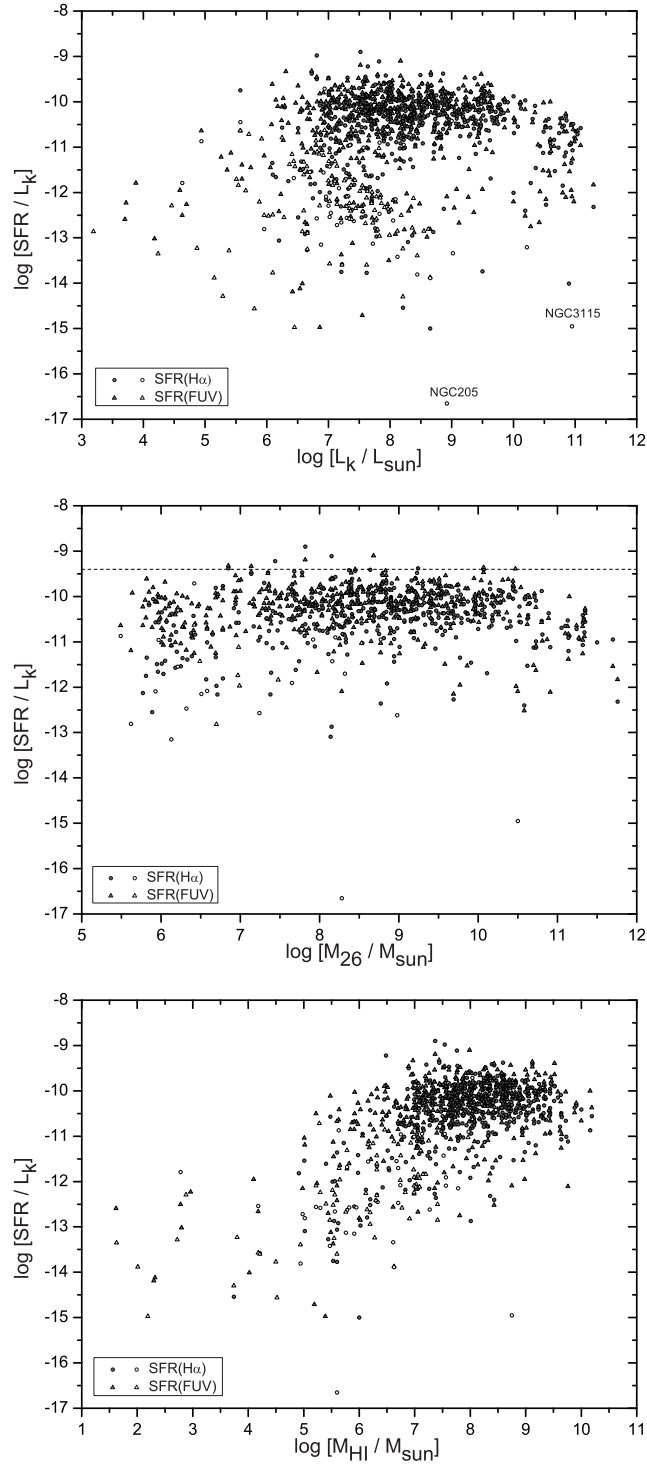


Fig. 4.— Specific star formation rates of nearby galaxies vs. their different global parameters: K_s -band luminosity (top panel), dynamical mass within the Holmberg diameter (middle panel), and total hydrogen mass (bottom panel). Circles are based on $H\alpha$ fluxes, triangles are based on FUV fluxes; open symbols correspond to the upper flux limits.

It should be emphasized again that the distribution of galaxies in this diagram is subjected to selection effects only in a minimal degree, as compared with other similar samples.

The middle panel of Fig. 4 shows the dependence of SSFR on the dynamic mass of a galaxy, determined within the Holmberg diameter by the amplitude of internal motions V_m . The shape of this diagram greatly differs from the top one, since the galaxies poor in neutral hydrogen are underrepresented here. The horizontal "Main Sequence" looks clearer here and shows the presence of an upper boundary $\log(SFR/L_K)_{max} \simeq -9.4$, above which there are just a few extremely blue peculiar galaxies: Garland, Mrk 209, Mrk 36, NGC 1592, UGCA 292.

Another parameter affecting the SFR is the total hydrogen mass of galaxy M_{HI} . As follows from the bottom panel of Fig. 4, the most rapid transformation of gas into stars occurs in the galaxies having large amount of neutral hydrogen. The slope of the log-log relationship between the SSFR and M_{HI} in the region of $\log(M_{HI}/M_\odot) < 7$ looks much steeper than in the galaxies with large hydrogen masses. A different nature of galaxy distribution in three panels of Fig. 4 again recalls that different conditions of galaxy selection in the considered sample by optical or HI features can greatly influence the shape and the subsequent interpretation of the observational data. This fact was also noted by Huang et al. (2012) when they compared the their samples, organized according to the ALFALFA, SDSS and GALEX survey data.

Fig. 5 presents the distribution of Local Volume galaxies according to their integral SFRs and total hydrogen masses. As one can see, the galaxies of different morphological types closely follow the known Schmidt-Kennicutt law with the slope of 3/2.

One of the most important global parameters of galaxies is their mean optical surface brightness, SB. The galaxies in the Local Volume have a scatter of mean surface brightnesses

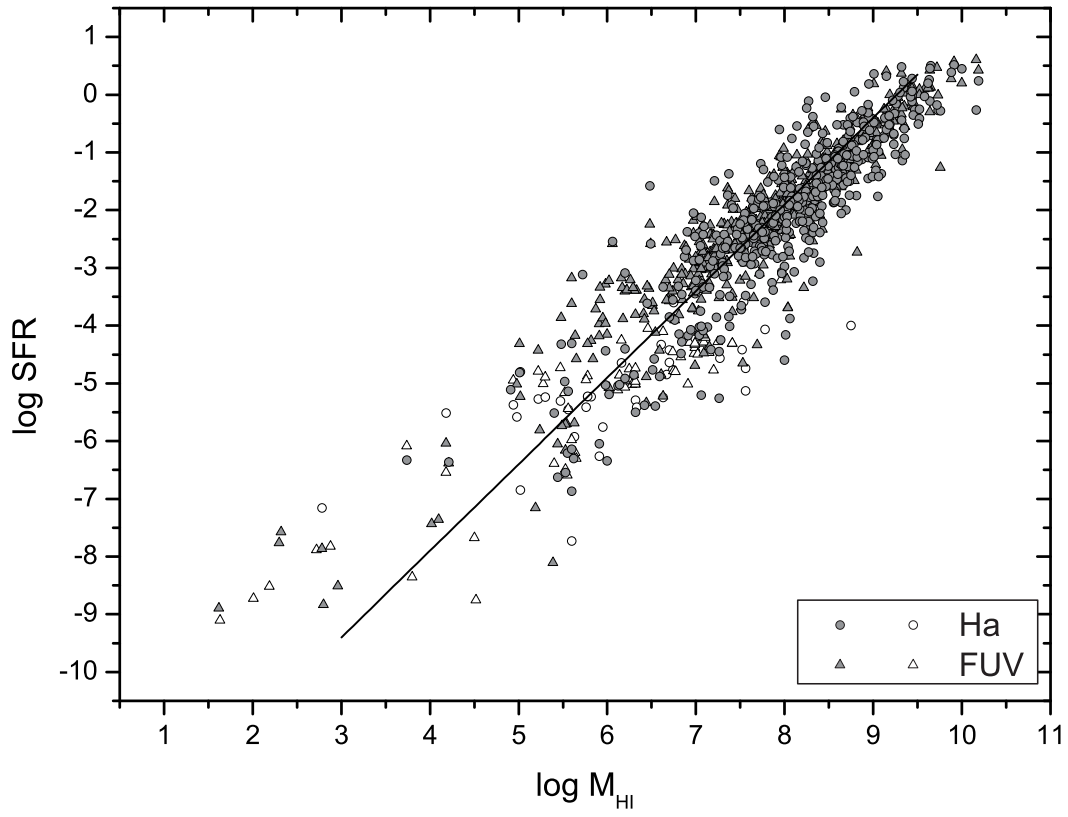


Fig. 5.— Integral SFR vs. total hydrogen mass for the Local Volume galaxies. Indication of galaxies with different SFR sources are the same as in Fig. 4. The solid line traces the slope 3/2 corresponding to the Schmidt-Kennicutt law.

in the B-band in the range of 21 to 30 mag arcsec⁻². Such enormous differences can significantly affect the efficiency and rate of star formation in the galaxies (Boissier et al. 2008, Meurer et al. 2009). The upper panel of Fig. 6 shows the relative SFR per L_B -luminosity unit of a given galaxy, determined by its $H\alpha$ flux depending on the surface brightness. As follows from this diagram, the specific star formation rate is almost not correlated with the surface brightness of the galaxy up to the value of SB \simeq 26.5 mag arcsec⁻². The SFR estimates by the FUV flux (the bottom panel of Fig. 6) extend into the region of fainter surface brightnesses, where there is a tendency of a declining specific star formation rate at SB > 26.5 mag arcsec⁻². A comparison of the upper and lower panels shows that the upper limit of SFR/ L_B looks sharper for the FUV fluxes. This feature can be explained by the fact that the $H\alpha$ flux characterizes the activity of star formation on a shorter time scale and hence its reaction to the bursts of star formation is less robust than that of the FUV flux.

5. SFR and dwarf morphology

Around 75% of the Local Volume population are dwarf galaxies with luminosities and sizes smaller than that of the Large Magellanic Cloud. In the de Vaucouleurs morphological classification they correspond to two types: T = 9 (irregular magellanic = Im, blue compact dwarf = BCD) and T = 10 (dwarf irregular = Ir). Moreover, dwarf elliptical galaxies — dE and diffuse spheroidals — Sph are usually added to the normal elliptical (E) and lenticular (S0) galaxies, being attributed the types T < 1. The shortcomings of such a simplified classification of dwarf systems have become apparent, hence, van den Bergh (1959) proposed a more refined scheme where dwarf galaxies assumed to be vary by luminosity classes.

In the UNGC, we have used a two-dimensional classification of dwarfs based on the available observational characteristics. In the vertical direction of our scheme, presented in

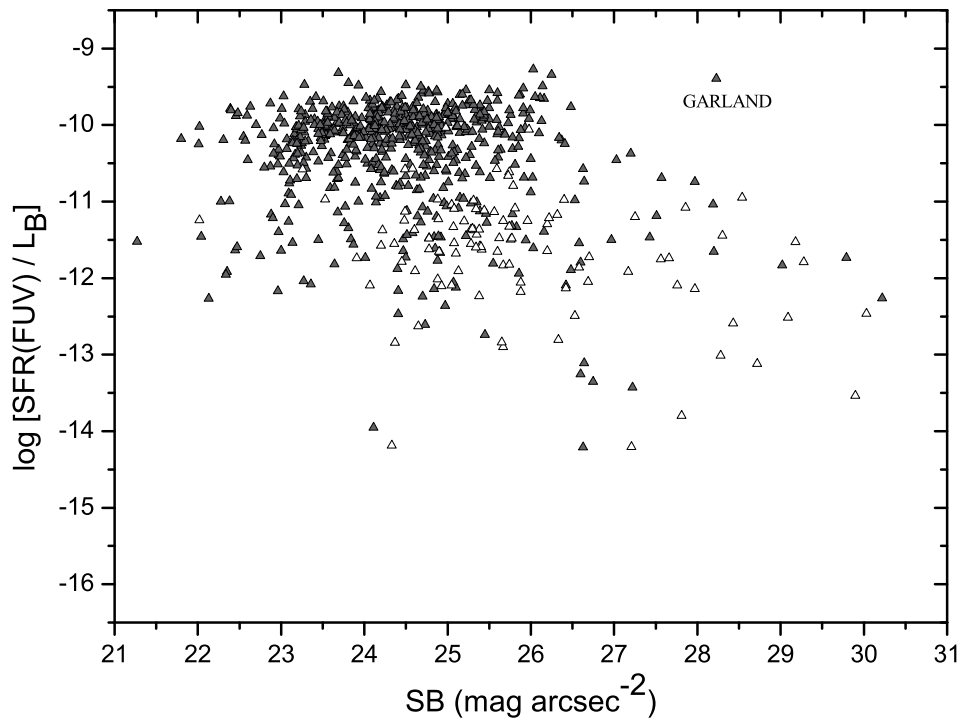
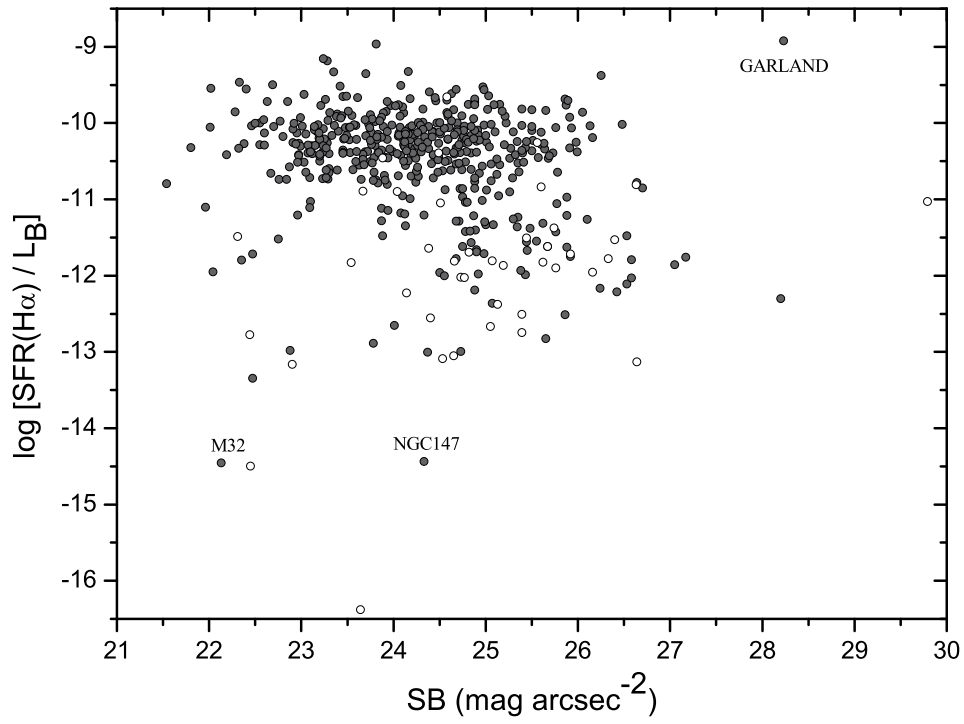


Fig. 6.— Specific star formation rate of nearby galaxies vs. their blue surface brightness. The top panel is derived from the $H\alpha$ imaging data, and the bottom panel — from FUV GALEX survey.

Table 1, dwarf galaxies varied in surface brightness gradations, the typical values of which amounted to: 23.0 — High SB, 24.2 — Normal SB, 25.2 — Low SB and 27.6 — eXtremely low SB, in units of [mag arcsec⁻²]. In the horizontal direction we have divided dwarf galaxies into red (old), intermediate, and blue (young). The first category are spheroidal (Sph), dwarf lenticular (dS0) and dwarf elliptical (dE) galaxies, as well as intergalactic globular clusters (gc). The second group are the objects of mixed stellar population Sph/Ir (or Transition), as well as the dE and dS0 dwarfs with emission spectra. The right column combines the dwarf system of BCD, Im, Ir types, as well as the rare cases of intergalactic HI-clouds with no signs of star formation. Such an approach allowed us to avoid unpleasant cases when a dwarf galaxy of intermediate type could jump over due to a misclassification from one end of de Vaucouleurs sequence ($T < 1$) to another one ($T = 9, 10$).

The bold numbers in Table 1 show how the Local Volume dwarfs are distributed by the cells of our two-dimensional scheme. The population of cells appears to be very uneven, which is caused both by the natural causes and the effects of observational selection.

For the dwarf galaxies belonging to each cell of Table 1, we have determined the average color indices $\langle m_{FUV} - B \rangle$, $\langle B - m_{H\alpha} \rangle$ and $\langle B - m_{21} \rangle$, corrected for the Galactic and internal extinction. Here, the apparent magnitudes were expressed through the corresponding fluxes as

$$\begin{aligned}
 m_{FUV} &= 23.90 - 2.5 \log F_{FUV} [mJy], \\
 m_{H\alpha} &= -13.64 - 2.5 \log F_{H\alpha} [erg \cdot cm^{-2} \cdot s^{-1}], \\
 m_{21} &= 17.4 - 2.5 \log F_{HI} [Jy \cdot km \cdot s^{-1}].
 \end{aligned}$$

The average value for each color index, standard deviation and the number of galaxies with the above attributes are presented in the cells of Table 2, which are identical to the

corresponding cells in Table 1. An analysis of these data reveals the following features.

In each subtype of surface brightnesses of dwarf galaxies where there exists a sufficient statistics, the average color index $\langle m_{FUV} - B \rangle$ increases towards blue \rightarrow mixed \rightarrow red. There is also a tendency of an increasing color index dispersion in the same direction.

In the transition from blue to red dwarfs, the average color indices $\langle B - m_{H\alpha} \rangle$ and $\langle B - m_{21} \rangle$ are systematically decreasing, which indicates a relative weakening of the emission in the $H\alpha$ and HI lines. The dispersion of the color indices tends to grow from blue to old red objects too.

The transition from dwarf galaxies of high surface brightness to the low and extremely low surface brightness has little effect on the average color index $\langle m_{FUV} - B \rangle$. For the red dwarfs the value of $\langle B - m_{H\alpha} \rangle$ increases, while for the blue dwarfs it decreases towards the objects of low surface brightness. The color index $\langle B - m_{21} \rangle$ grows from compact dwarfs to extremely diffuse dwarfs, indicating that the proportion of gas relative to the stellar mass is greater in the latter galaxies.

6. Starbursts in low-mass galaxies

The literature repeatedly expressed concerns that the conversion of gas into stars in dwarf galaxies has a oscillatory, starburst character (Dohm-Palmer et al. 2002, Skillman 2005, McConnachie et al. 2006, Karachentsev & Kaisin 2007, McQuinn et al. 2009). Stinson et al. (2007) performed a numerical simulation of this process and have shown that in gas-rich dwarf galaxies with masses of $\log(M/M_{\odot}) < 9$ the bursts of star formation can vary the SFRs severalfold on the typical time scale of $\sim 3 \cdot 10^8$ years. According to the models of periodic SFH for dwarf galaxies, considered by Weisz et al. (2012), the low-mass galaxies increase their SFRs by a factor of 10 -50 over the average SFR during the

inter-burst period. Their burst duration and cycle periods are typically tens of Myr and 200 - 300 Myr, respectively. The same variability, determined by the internal parameters of a dwarf galaxy itself is superimposed by some external factors: the excitation of star formation activity due to the tidal effects from a massive neighboring galaxy, as well as the sweeping out gas from the dwarf system as it passes through the dense regions of its massive neighbor. The relative role of external and internal factors, affecting the evolution of a given dwarf galaxy should evidently depend on the density of its environment.

Panels of Fig. 7 show the distribution of dwarf galaxies with stellar masses $\log(M_*/M_\odot) < 9$ by the SSFR depending on their environment. The galaxies with SFR estimated from the $H\alpha$ flux and FUV flux are depicted by the circles and triangles, respectively. The upper limits of the flux are shown by empty symbols. The horizontal axis of the top panel represents the so-called "tidal index" of a galaxy

$$\Theta_1 = \max[\log(M_n/D_n^3)] - 10.96, \quad n = 1, 2 \dots N$$

which is expressed in terms of mass M_n and spatial distance D_n of the most significant neighboring galaxy (Karachentsev et al. 2013). Positive values of Θ_1 correspond to the members of groups, and negative — to the field galaxies. The bottom panel uses another dimensionless indicator as an argument,

$$\Theta_j = \log[j_K(1\text{Mpc})/j_{K,global}],$$

which characterizes the contrast of stellar density around the considered galaxy in a sphere with a 1 Mpc radius, expressed in the units of global mean density $j_{K,global} = 4.28 \cdot 10^8 L_\odot \text{Mpc}^{-3}$ (Jones et al. 2006). For extremely isolated galaxies with no neighbors within 1 Mpc, the values of Θ_j are formally accepted by us to amount to -3 .

As follows from the data presented, the smallest scatter in the specific star formation rate is found in isolated dwarf galaxies. In high density regions, $\Theta_1 > 0$ or $\Theta_j > 1$,

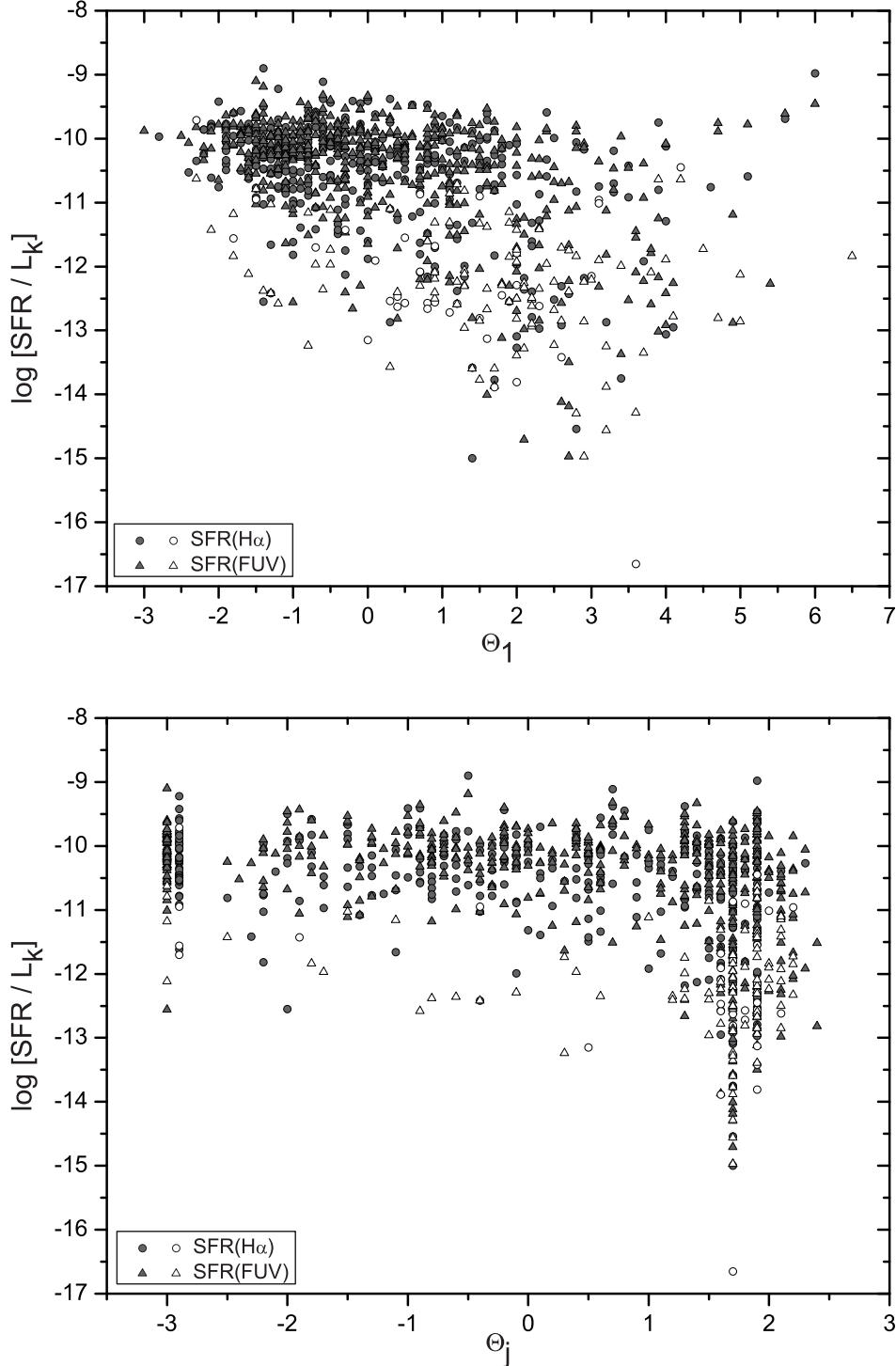


Fig. 7.— Specific star formation rate for the dwarf ($\log M_* < 9$) Local Volume galaxies as a function of two environment parameters: Θ_1 , determined by the nearest significant neighbor (top panel), and Θ_j , indicating the stellar mass density contrast within the 1 Mpc radius in the units of mean global density (bottom panel). Symbols are the same as in Fig. 4 - Fig. 6. Negative values of Θ correspond to the field galaxies, while positive ones correspond to the group members.

there is a noticeable amount of dwarf objects with depressed star formation rates $\log(SFR/M_*) < -11.5$. Their relative number is not too significant, only $\sim 15\%$, but this figure may be seriously biased by the effects of observational selection. Note also that at the level of highest SSFR values, we practically do not recognize any dwarf galaxies, in which an increase in the SFR would be triggered by a dense neighborhood. A rare and outstanding example of this is "Garland" — a dwarf galaxy at the NGC 3077 periphery, which looks like a chain of emission HII-regions, immersed in a cloud of molecular hydrogen (Karachentsev et al. 1985, Walter et al. 2002).

Globally, the data presented in Fig. 7 show that in the majority of dwarf galaxies, the rates of transformation of gas into stars are largely determined by the internal processes rather than any external effects.

To characterize the evolutionary status of a sample of galaxies, Karachentsev & Kaisin (2007) proposed to use a diagnostic "past-future" (=PF) diagram, where the dimensionless parameters

$$P = \log(SFR \cdot T_0 / L_K),$$

$$F = \log(1.85 \cdot M_{HI} / SFR \cdot T_0)$$

are independent of errors in finding distances to the galaxies. The parameter P is actually the specific star formation rate over the entire age scale of the universe, $T_0 = 13.7$ Gyr. The F parameter corresponds to the notion of gas depletion time, expressed in the units of T_0 . The coefficient of 1.85 at M_{HI} is introduced in order to account for the contribution of helium and molecular hydrogen in the total mass of gas (Fukugita & Peebles 2004).

The summary of observational data on the integral SFR (columns 5 and 8) and evolutionary parameters $\{P, F\}$ (columns 6,7 and 9,10) for 802 galaxies of the Local Volume is given in Table 3. The first two columns contain the name of the galaxy and its equatorial coordinates, the third column indicates the galaxy morphology by de Vaucouleurs scale,

and the fourth column lists the B-band absolute magnitude corrected for the Galactic and internal extinction.

Figure 8 reproduces the diagnostic diagrams of $\{P, F\}$ for the early-type $T < 2$ galaxies of the Local Volume (the top panel), for the spiral galaxy types $T = (2-8)$ (middle panel) and dwarf galaxy types $T=(9,10)$ (the bottom panel).

The top panel shows that in the E and S0 galaxies, the current star formation rates are by 2–3 orders of magnitude lower than the earlier rates, which formed the observed stellar mass of these galaxies. Given the present reserves of gas, their observed "glowing" star formation rates can be maintained at the average on the scale of several more Hubble times.

As follows from the middle panel, a typical spiral galaxy has time to reproduce its stellar mass at its observing SFR. The gas reserves in a typical spiral are enough to keep the current rate of gas conversion into stars on a scale of ~ 10 Gyr. In other words, the disks of galaxies act as rhythmic stellar factories and are yet located half way of their evolution. The farthest distance from the origin $P = 0, F = 0$ is shown by the galaxy NGC 1569, which reveals a burst of star formation in the central region and radial expansion of emission filaments (Israel 1988, Hodge 1974).

The data on the bottom panel demonstrate that the majority of dwarf Ir, Im, BCD galaxies, the same as the spirals, reproduce their stellar mass at the current SFR values. The gas reserves in a typical representative of this population are sufficient to maintain the average observed SFR level for several more Hubble times. In this sense, the secular evolution of the late-type dwarfs can be characterized as inhibited, or "lethargic" evolution.

Apart from the main concentration of dwarf galaxies near the origin $P = 0, F = 0$, about a quarter of the population of Ir, Im, BCD-dwarfs reveal an elongation along the diagonal of $F = -P$. This effect is easily explained by the assumption that a part of the

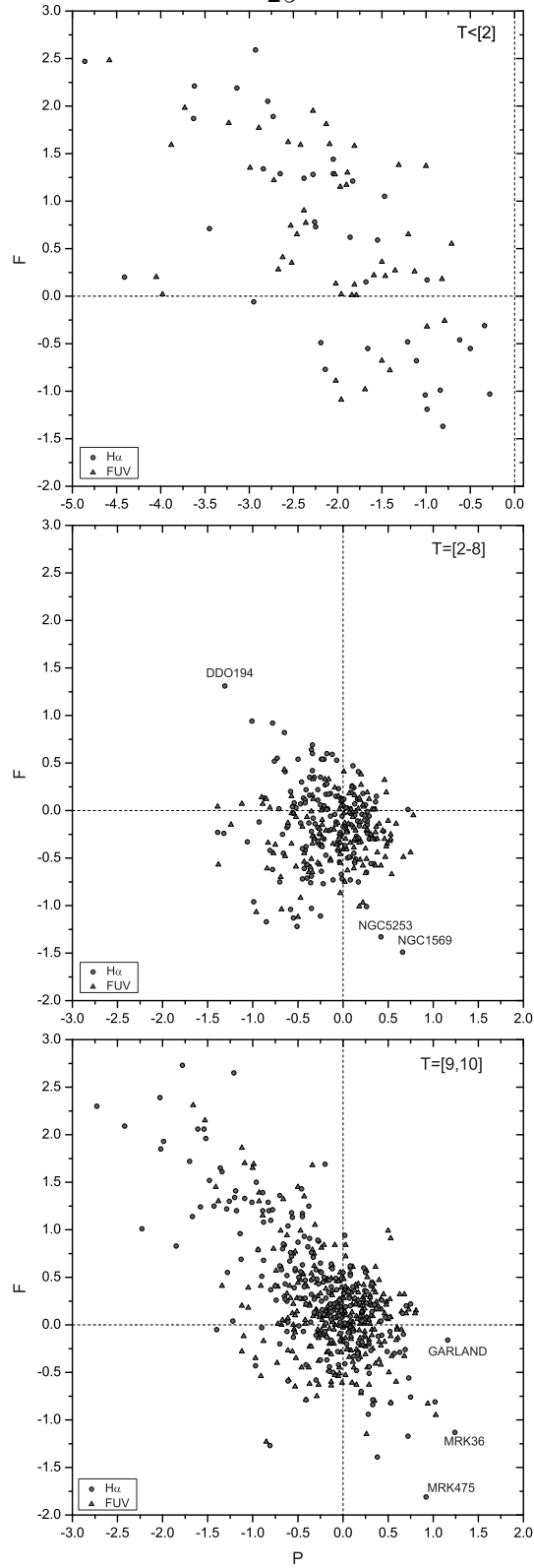


Fig. 8.— The diagnostic "past-future" diagram for the early-type (E,S0, dSph) galaxies (top panel), spiral galaxies (middle panel), and late-type (BCD, Im, Ir) dwarfs (bottom panel).

dwarf population is in a starburst state, which is then followed by a more prolonged star formation depression stage. Statistics of starbursting dwarfs in the right bottom corner of the bottom panel tells us that only $\sim 1/20$ part of the total amount of dwarf galaxies are experiencing vigorous bursts. This result is fully consistent with the conclusion by Lee et al. (2009) that "dwarfs that are currently experiencing massive global bursts are just the $\sim 6\%$ tip of a low-mass galaxy iceberg". Table 4 lists 15 most representative starburst-state galaxies. Its columns contain: (1) — the name of the active galaxy, (2-3) — the P parameter obtained from the $H\alpha$ and FUV fluxes, (4) — morphology, (5) — absolute B-magnitude, (6) — tidal index. The most extreme P values are observed in dwarfs with SFR estimates from the $H\alpha$ flux. This situation fits into the general concept of the recurrent starburst activity of low-mass galaxies, since the $H\alpha$ fluxes fix the SFR value at a shorter term ($\sim 10^7$ Myr), than the FUV fluxes do ($\sim 10^8$ Myr).

The data of Table 4 again show that the starbursts depend little on the galaxy neighborhood density.

7. Concluding remarks

We have discussed the available observational data on the current rate of star formation in the galaxies with distances of $D < 11$ Mpc, which was determined from the integral flux of galaxy in the emission $H\alpha$ line or from the FUV flux, obtained at the GALEX orbital telescope. Our sample of galaxies has two advantages: 1) it is the most representative of all the existing samples in the Local Volume, 2) at its formation we have not used any restrictions on the morphological properties of galaxies. About 3/4 of the sample are dwarf galaxies that we have classified by the gradations of surface brightness and color.

The population of dwarf galaxies shows signs of stochastic starburst activity, which

scatters them on the diagnostic $\{P, F\}$ diagram along the diagonal of $F = -P$. On the average, blue dwarf galaxies (Ir, Im, BCD) possess current star formation rates, sufficient to regenerate their observed stellar masses, and their gas reserves allow them to maintain the observed average SFR on the scale of several Hubble times. This statement does not apply to the dwarf spheroidal companions that have lost their gas component passing through the dense regions of massive neighboring galaxies.

Spiral galaxies of Sa–Sm types (T=2–8) on average have about the same specific rate of star formation as the Ir, Im and BCD dwarf systems. Their dispersion in the $\{P, F\}$ diagram is much smaller than that of dwarfs. Apparently, the disks of spiral galaxies convert gas into stars in a regular fashion, which is determined by purely internal mechanisms with a small influence of the external environment.

For the Local Volume galaxies of different morphological types there exists an upper limit of the specific star formation rate, $\log(SFR/M_*)_{lim} \simeq -9.4$ [yr^{-1}], to which corresponds the dimensionless parameter $P_{lim} \simeq 0.75$. Above this limit, there are only a few ($\sim 1\%$) low-mass galaxies that fall into this region in the state of a short vigorous starburst, or due to uncertainty in the estimates of their SFR and P (compare the data on P in columns (2) and (3) of Table 4). The presence of this $\log(SFR/M_*)_{lim} = -9.4$ limit is well seen in Fig.9 by Schiminovich et al. (2010) for a sample of 190 massive HI- selected galaxies from Arecibo SDSS & GALEX survey. Recently, just the same upper limit was also found for a sample of 500 local isolated galaxies and a sample of 270 nearby Markarian galaxies (Karachentsev et al. 2013b). The derived upper limit in specific star formation rate deserves attention of theoreticians. It may indicate that the conversion of gas into stars is regulated by a rather rigid feedback, when an excessively active star formation rate is blocked by the depletion of internal resources for it.

The population of E, S0 and dSph galaxies in the Local Volume is characterized by

very low rates of star formation. To reproduce the observed stellar mass of these galaxies, their average SFR in the past should have been tens to hundreds of times higher than the one observed now. It should be noted, however, that these arguments suggest the evolution of galaxies within the "closed box" scheme. There are ample evidence that galaxies increase their mass with time by the accretion of baryonic matter from the intergalactic space (Marinacci et al. 2010, Cattaneo et al. 2011). The presence of the isolated E and S0 galaxies: NGC 404, NGC 855 and NGC 4600 with active emission nuclei (Moiseev et al. 2010) in the Local Volume may serve as a confirmation of the fact that the process of accretion of intergalactic baryons was at work not solely a long time ago, but it also extends into the present epoch.

The authors are grateful to the referee for the comments that have improved the paper. We thank Dmitry Makarov for the useful discussions. This work was supported in part by the RFBR grants no. 12-02-91338 and 13-02-92690. We acknowledge the support for proposals GO 12546, 12877, 12878, which was provided by the NASA through grants of the Space Telescope Science Institute. This research has made use of the survey web services of the NASA/IRAC Extragalactic Database (NED) and the Galaxy Evolution Explorer (GALEX).

REFERENCES

- Bell E.F., McIntosh D.H., Katz N., & Weinberg M.D., 2003, *ApJS*, 149, 289
- Boissier S., Gil de Paz A., Boselli A., et al. 2008, *ApJ*, 681, 244
- Bouchard A., Da Costa G.S., & Jerjen H., 2009 *AJ*, 137, 3038
- Cattaneo A., Mamon G.A., Warnick K., & Knebe A., 2011, *A & A*, 533, 5
- Dohm-Palmer R.C., Skillman E.D., Mateo M., et al. 2002, *AJ*, 123, 813
- Epinat B., Amram P., & Marcelin M., 2008, *MNRAS*, 390, 466
- Fukugita M., & Peebles P.J.E., 2004, *ApJ*, 616, 643
- Fumagalli M., Da Silva R.L. & Krumholz M.R., 2011, *ApJL*, 741, L25
- Gil de Paz A., Madore B.F. & Pevunova O. 2003, *ApJS*, 147, 29
- Gil de Paz A., Boissier S., Madore B.F. et al. 2007, *ApJS*, 173, 185
- Hodge P.W., 1974, *ApJ*, 191L, 21
- Huang S., Haynes M.P., Giovanelli R., & Brinchmann J., 2012, *ApJ*, 756, 113
- Hunter D.A., Elmegreen B.G., & Ludka B.C., 2010, *AJ*, 139, 447
- Hunter D.A. & Elmegreen B.G. 2004, *AJ*, 128, 2170
- Israel F.P., 1988, *A & A*, 194, 241
- James, P. A., Shane, N. S., Beckman, J. E. et al., 2004, *A & A*, 414, 23
- James P.A., Knapen J.H., Shane N.S. et al., 2008, *A & A*, 482, 507
- Jones D.H., Peterson B.A., Colless M., & Saunders, W., 2006, *MNRAS*, 369, 25

- Kaisin S.S., Kasparova A.V., Kniazev A.Yu., & Karachentsev I.D., 2007, *Astron. Lett.*, 33, 1
- Kaisin S.S., & Karachentsev I.D., 2006, *Astrofizika*, 49, 337
- Kaisin S.S., & Karachentsev I.D., 2008, *A&A*, 479, 603
- Kaisin S.S., Karachentsev I.D., & Kaisina E.I., 2011, *Astrofizika*, 54, 353
- Kaisina E.I., Makarov D.I., Karachentsev I.D., & Kaisin S.S., 2012, *AstBul*, 67, 115
- Karachentsev I.D., Karachentseva V.E., & Borngen F., 1985, *MNRAS*, 217, 731
- Karachentsev I.D., Kaisin S.S., Tsvetanov Z., & Ford H., 2005, *A&A*, 434, 935
- Karachentsev I.D., & Kaisin S.S., 2007, *AJ*, 133, 1883
- Karachentsev I.D., & Kaisin S.S., 2010, *AJ*, 140, 1241
- Karachentsev I.D., Kaisina E.I., Kaisin S.S., & Makarova L.N., 2011, *MNRAS*, 415L, 31
- Karachentsev I.D., Makarov D.I., & Kaisina E.I., 2013a, *AJ*, 145, 101
- Karachentsev I.D., Karachentseva V.E., & Melnyk O.V., 2013b, *Astroph Bull*, 68 (accepted)
- Kennicutt R.C. & Evans N.J., 2012, *ARAA*, 50, 531
- Kennicutt R.C., 1998, *ARA&A*, 36, 189
- Kennicutt R.C., Lee J.C., Funes J.G. et al., 2008, *ApJS*, 178, 247
- Lee J.C., Gil de Paz A., Kennicutt R.C., et al. 2011, *ApJS*, 192, 6
- Lee J.C., Kennicutt R.C., Funes J.G. et al., 2009, *ApJ*, 692, 1305
- Marinacci F., Binney J., Fraternali F., et al. 2010, *MNRAS*, 404, 1464
- McConnachie A.W., Arimoto N., Irwin M., & Tolstoy E., 2006, *MNRAS*, 373, 715

- McQuinn K.B., Skillman E.D., Cannon J.M., et al. 2009, ApJ, 695, 561
- Meuer G.R., Wong O.I., Kim J.H. et al. 2009, ApJ, 695, 765
- Meurer G.R., Hanish D.J., Ferguson H.C., et al. 2006, ApJS, 165, 307
- Moiseev A.V., Karachentsev I.D.,& Kaisin S.S., 2010, MNRAS, 403, 1849
- Pflamm-Altenburg J., Weidner C.,& Kroupa P., 2009, MNRAS, 395, 394
- Pflamm-Altenburg J., Weidner C.,& Kroupa P., 2007,ApJ, 671, 1550
- Relano M., Kennicutt R.C., Eldridge J.J., et al., 2012, MNRAS, 423, 2933
- Schiminovich D., Catinella B., Kauffmann G. et al. 2010, 408, 919
- Schlegel D.J., Finkbeiner D.P., & Davis M., 1998, ApJ, 500, 525
- Skillman E.D., 2005, New Astronomy survey, 49, 453
- Stinson G.S., Dalcanton J.J., Quinn T., et al. 2007, ApJ, 667, 170
- Tully R.B., Shaya E.J., Karachentsev I.D. et al., 2008, ApJ, 676, 184
- Tully R.B.,& Fisher R.J., 1977, A & A, 54, 661
- van den Bergh S., 1959, Publ. David Dunlap Obs., 2, 14
- Verheijen, M.A.W., 2001, ApJ, 563, 694
- Walter F., Weiss A., Martin C.,& Scoville N., 2002, AJ, 123, 225
- Weisz D.R., Johnson B.D., Johnson L.C., et al. 2012, ApJ, 744, 44
- Young J.S., Allen L., Kenny J.D. et al., 1996, AJ, 112, 1903

Table 1: Classification for dwarf galaxies

High	2 dE, gc	1 dEem	13 BCD
Normal	23 dS0,Sph	15 dS0em,Tr	320 BCD,Im,Ir
Low	60 Sph	43 Ir/Sph,Tr	115 Ir
X-Low	49 Sph	4 Tr	6 Ir,HI cld
↑ SB	Red Gas content →	Mixed	Blue ← Color Index

Table 2: Average colors for different dwarf types

Color	SB	Red			Mixed			Blue		
		$\langle \rangle$	σ	n	$\langle \rangle$	σ	n	$\langle \rangle$	σ	n
$m_{FUV} - B$	H	4.93	0.35	2	–	–	1	1.57	0.79	9
	N	6.07	1.90	17	4.41	1.34	14	1.72	0.96	260
	L	5.64	1.63	51	4.84	1.52	42	2.26	1.41	87
	X	5.98	2.73	44	4.53	3.02	3	1.55	1.58	2
$B - m_{H\alpha}$	H	–	–	0	–	–	1	–2.96	1.45	5
	N	–11.07	5.15	5	–5.84	2.43	7	–4.31	1.48	153
	L	–8.36	1.69	21	–7.80	1.08	12	–5.19	1.90	50
	X	–7.75	1.93	6	–	–	0	–	–	1
$B - m_{21}$	H	–	–	1	–	–	1	–2.17	0.97	9
	N	–3.23	3.84	8	–2.19	1.16	12	–0.79	1.11	230
	L	–2.20	1.94	31	–1.68	1.51	30	0.01	1.05	78
	X	–2.34	3.18	26	–	–	1	0.17	1.46	2

Table 3. List of the nearby galaxies with measured SFR

Galaxy	RA (J2000.0)	Dec.	T	M_B	$SFR_{H\alpha}$	$P_{H\alpha}$	$F_{H\alpha}$	SFR_{FUV}	P_{FUV}	F_{FUV}
1	2	3	4	5	6	7	8	9	10	
UGC12894	000022.5+392944		10	-13.31	-2.48	0.08	0.53	-2.03	0.53	0.08
WLM	000158.1-152740		9	-14.06	-2.69	-0.24	0.65	-2.24	0.21	0.20
And XVIII	000214.5+450520		-3	-9.11				< -5.81	< -2.27	
ESO409-015	000531.8-280553		9	-14.35	-1.57	0.57	-0.31	-1.82	0.32	-0.06
AGC748778	000634.4+153039		10	-10.04				-3.65	0.22	0.29
And XX	000730.7+350756		-3	-5.77				-5.96	-1.08	
UGC00064	000744.0+405232		10	-14.75				-1.63	0.35	0.34
ESO349-031	000813.3-343442		10	-11.87	-4.03	-1.01	1.29	-3.02	0.00	0.28
NGC0024	000956.4-245748		5	-18.32	-0.74	-0.35	-0.22	-0.34	0.05	-0.62
NGC0045	001403.9-231056		8	-18.53	-0.26	0.27	-0.14	-0.17	0.36	-0.23
NGC0055	001508.5-391313		8	-18.41	-0.35	0.30	-0.07	-0.21	0.44	-0.21
NGC0059	001525.1-212638		-3	-15.74	-1.91	-0.50	-0.56	-2.20	-0.79	-0.27
ESO410-005	001531.4-321048		10	-11.58	< -6.26	< -3.01	>2.30	-3.97	-0.72	0.01
And XIX	001932.1+350237		-3	-8.32				< -6.27	< -2.41	
IC0010	002024.5+591730		10	-15.99	-1.54	0.12	-0.33			
And XXVI	002345.6+475458		-3	-6.47				< -6.30	< -1.70	
Sc22	002351.7-244218		-3	-10.46	< -5.58	< -2.58	>0.69	-5.02	-2.02	0.13
Cetus	002611.0-110240		-1	-10.18	< -5.51	< -2.40	> -0.18	< -6.54	< -3.43	>0.85
ESO294-010	002633.3-415120		10	-10.91	-4.32	-0.43	-0.07	-3.86	0.03	-0.53
UGC00288	002904.0+432554		10	-13.83	-2.62	-0.27	0.43	-2.34	0.01	0.15

Note. Only a portion of this table is shown here to demonstrate its form and content.

Machine-readable version of the full table is available.

Table 4: The most active galaxies in the Local Volume

Name	$P_{H\alpha}$	P_{FUV}	T	M_B	Θ_1
(1)	(2)	(3)	(4)	(5)	(6)
Mrk 36	1.24	0.94	BCD	−14.04	−1.4
NGC1592	–	1.03	Ir	−15.50	−1.5
Garland	1.15	0.68	Ir	−11.40	6.0
DDO 169NW	–	0.80	Ir	−10.16	0.0
Mrk 209	1.02	0.54	Ir	−13.69	−0.6
UGCA 292	0.75	0.81	Ir	−11.79	−0.6
NGC4597	0.73	0.78	Sdm	−17.81	0.0
NGC5408	0.73	–	Im	−16.51	−0.2
DDO 143	0.70	0.73	Ir	−13.88	−0.5
UGC4483	0.67	0.65	Ir	−12.73	0.6
GR 8	0.63	0.68	Ir	−11.96	−1.4
UGC6456	0.70	0.60	Ir	−14.08	−0.1
DDO 53	0.66	0.60	Ir	−13.37	0.8
NGC4861	0.76	0.43	Im	−16.52	0.3
Mrk 475	0.92	0.26	BCD	−13.46	−1.2